[CANCER RESEARCH 64, 7553–7561, October 15, 2004]

Treatment-Induced Changes in Tumor Oxygenation Predict Photodynamic Therapy Outcome

Hsing-Wen Wang,[1,3] Mary E. Putt,[2] Michael J. Emanuele,[3] Daniel B. Shin,[3] Eli Glatstein,[3] Arjun G. Yodh,[1] and Theresa M. Busch[3]

Departments of [1]Physics and Astronomy, [2]Biostatistics and Epidemiology, and [3]Radiation Oncology, University of Pennsylvania, Philadelphia, Pennsylvania

ABSTRACT

Photodynamic therapy (PDT) requires oxygen to cause tumor damage, yet therapy itself can deplete or enhance tumor oxygenation. In the present work we measured the PDT-induced change in tumor oxygenation and explored its utility for predicting long-term response to treatment. The tissue hemoglobin oxygen saturation (SO_2) of murine tumors was noninvasively measured by broadband diffuse reflectance spectroscopy. In initial validation studies, the oxyhemoglobin dissociation curve for mouse blood was accurately recreated based on measurements during deoxygenation of a tissue phantom of mouse erythrocytes. *In vivo* studies exhibited excellent correlation between carbogen-induced changes in SO_2 and pO_2 of radiation-induced fibrosarcoma tumors measured by reflectance spectroscopy and the Eppendorf pO_2 histograph, respectively. In PDT studies radiation-induced fibrosarcoma tumor SO_2 was measured immediately before and after Photofrin-PDT (135 J/cm^2, 38 mW/cm^2). Animals were subsequently followed for tumor growth to a volume of 400 mm^3 (time-to-400 mm^3) or the presence of tumor cure (no tumor growth at 90 days after treatment). In animals that recurred, the PDT-induced change in tumor SO_2, *i.e.*, relative-SO_2 (SO_2 after PDT/SO_2 before PDT) was positively correlated with treatment durability (time-to-400 mm^3). The predictive value of relative-SO_2 was confirmed in a second group of animals with enhanced pre-PDT oxygenation due to carbogen breathing. Furthermore, when all of the animals were considered (those that recurred and those that were cured) a highly significant association was found between increasing relative-SO_2 and increasing probability of survival, *i.e.*, absence of recurrence. As independent variables, the SO_2 after PDT, the pre-PDT tumor volume, and light penetration depth all failed to predict response. As an independent variable, the SO_2 before PDT demonstrated a weak negative association with treatment durability; this association was driven by a correlation between decreasing pre-PDT SO_2 and increasing relative-SO_2. These data suggest that monitoring of PDT-induced changes in tumor oxygenation may be a valuable prognostic indicator.

INTRODUCTION

Oxygen is an essential component of photodynamic therapy (PDT). As it is commonly applied in oncology, PDT involves the administration of a photosensitizer followed by the exposure of tumor to light of a specific wavelength (1). The light-excited photosensitizer interacts with ground state oxygen to form oxidized products and/or singlet oxygen, causing tissue destruction through a combination of mechanisms, including direct cytotoxicity, vascular damage, and stimulation of host immune responses. PDT can deplete oxygenation during treatment through photochemical oxygen consumption and reversible or irreversible reductions in blood vessel perfusion (2–6). However, the effect of PDT on tumor oxygenation is highly dependent on choice of photosensitizer, drug-light interval, and fluence rate. Others, for example, have found PDT to enhance tumor oxygenation during and immediately after illumination, perhaps through increased vascular perfusion and/or decreased oxygen consumption due to tumor cell death (7, 8). Oxygen-favoring PDT protocols lead to more durable tumor responses in preclinical models (9–11). Accordingly, *in vivo* monitoring of tumor oxygen levels before, during, and after PDT may have great clinical significance.

Methods for studying tumor oxygenation during or after PDT include invasive measurements by oxygen-sensitive needle electrodes, electron paramagnetic resonance oximetry, and hypoxia marker binding. The Eppendorf pO_2 histograph, a 300 μm-diameter polarographic needle probe, as well as smaller microelectrodes have been used to measure tumor oxygenation before, during, and after PDT (4–6, 8, 12). In electron paramagnetic resonance oximetry, synthetic oxygen-sensitive particles (lithium phthalocyanine, 50 to 200 μm) were implanted into the tissue of interest at $\geq$24 hours before treatment, and tumor pO_2 was monitored by an electron paramagnetic resonance spectrometer at selected time points (7, 13). Hypoxia markers, such as EF3 [2-(2-Nitroimidazol-1[H]-yl)-N-(3,3,3-trifluoropropyl)acetamide] and misonidazole, among others, have also been used to label tumor hypoxia during and after PDT (14–19). In most instances, the extent of hypoxia is measured by analysis of drug binding in excised tumor samples (14).

Few noninvasive techniques for measuring the oxygenation of PDT-treated tumors have been reported. Phosphorescence quenching spectroscopy is minimally invasive. It involves the i.v. injection of a phosphorescent compound, *e.g.*, palladium meso-tetra-(4-carboxyphenyl) porphine, which exhibits exponential O_2-dependent decay after a pulse excitation (20). Transcutaneous oxygen tension during PDT has been measured using Clark-type electrodes taped to skin carcinomas on the inside of rabbit ears (2). Finally, near-infrared photon-migration spectroscopy has been used to measure tissue concentrations of photosensitizing drug, hemoglobin, and hemoglobin oxygen saturation at several time points in relation to PDT (21). The advantages of noninvasive measurements include the ability to follow response in the same tumor over time and the comparative ease of applying noninvasive measurement techniques in the clinic.

In the present study, we use broadband diffuse reflectance spectroscopy to noninvasively measure the tumor hemoglobin oxygen saturation (SO_2) of radiation-induced fibrosarcoma tumors before and after PDT. Results demonstrate that PDT-induced changes in tumor SO_2 immediately after illumination relative to the pretreatment value (relative-SO_2) are significantly correlated with treatment response. Relative-SO_2 was predictive of treatment durability, defined as the number of days for post-treatment tumor growth to a volume of 400 mm^3. Furthermore, probability of survival, *i.e.*, probability of maintaining a tumor volume $<$400 mm^3 over the course of the study, was significantly improved in animals with higher relative-SO_2. These data suggest that knowledge of PDT-induced dynamics in tumor oxygenation is a valuable predictive tool of long-term PDT response.

MATERIALS AND METHODS

Animals and Tumor Model. Radiation-induced fibrosarcoma tumors were propagated on the shoulders of C3H mice (Taconic, Germantown, NY) by the intradermal injection of 3×10^5 cells (14) ~1 week before PDT treatment or

Received 11/19/03; revised 8/5/04; accepted 8/12/04.

Grant support: NIH PO1 grant CA87971 and RO1 grant CA85831.

The costs of publication of this article were defrayed in part by the payment of page charges. This article must therefore be hereby marked *advertisement* in accordance with 18 U.S.C. Section 1734 solely to indicate this fact.

Requests for reprints: Hsing-Wen Wang, Department of Radiation Oncology, B13 Anatomy and Chemistry Building, 3620 Hamilton Walk, Philadelphia, PA 19104-6072. E-mail: hwwang@physics.upenn.edu.

control illumination. PDT-treated tumors were ~4 to 5.5 mm in diameter, with a maximum volume of 100 mm^3 (tumor volume = diameter × width^2 × 3.14/6) at the time of treatment. Fur in the treatment area was removed with a shaver and a depilatory (Nair).

Photodynamic Therapy Treatment. The photosensitizer Photofrin (Axcan Pharma Inc., Mont-Saint-Hilaire, Quebec, Canada) was administered via tail vein at 5 mg/kg at ~24 hours before illumination. Light at 630 nm was produced by a KTP Yag pumped dye module (Laserscope, San Jose, CA) and delivered via a quartz fiber microlens. The laser output was measured with a power meter (Coherent, Auburn, CA) and adjusted to produce a fluence rate of 38 mW/cm^2 over a 1 cm-diameter field. All of the treatments were to a total fluence of 135 J/cm^2, requiring 60 minutes of illumination. Control animals that did not receive Photofrin were exposed to illumination at the same fluence rate and fluence. After PDT or control treatment, mice were followed daily to determine the day on which tumor volume equaled or exceeded 400 mm^3 (time-to-400 mm^3). A cure was defined as no tumor recurrence at 90 days after PDT. Beginning 5 to 15 minutes before until 5 minutes after illumination, animals were maintained under isoflurane anesthesia, inhaled via nosecone, to facilitate rapid measurement of tumor oxygenation immediately before and after light delivery (see Broadband Reflectance Spectroscopy, below). In indicated studies, carbogen (2 L/minutes) replaced medical air as the gas in the anesthetic mixture. Carbogen breathing was begun 15 minutes before the start of illumination and terminated after the post-PDT spectroscopy measurement.

Broadband Reflectance Spectroscopy. A continuous wave broadband reflectance spectroscopy system was used to measure tissue optical properties, including absorption (μ_a) and reduced scattering coefficients (μ_s'), in the spectral range 600 to 800 nm (22, 23). The system consisted of a 250 W quartz tungsten halogen lamp (Cuda Fiberoptics, Jacksonville, FL), a hand-held surface contact fiber-optic probe, a spectrograph (SpectraPro-150, Acton Research, Acton, MA), and a liquid nitrogen cooled CCD camera (LN/CCD-1100-PF/UV, Roper Scientific, Trenton, NJ) to image the reflectance spectra from multiple detection fibers simultaneously. To account for the spectral features of the white light source and the optical throughput of our detection system, the reflectance spectra was calibrated based on measurements in a 6-inch diameter integrating sphere (ref. 23; LabSphere Inc., North Sutton, NH). The fiber-optic probe consisted of a 400 μm-diameter source fiber and 10 colinear 400 μm-diameter detection fibers at various source-detector separation distances. Source-detector separation distances between 1.2 mm and 4 mm were typically used, depending on the diameter and curvature of the tumor surface. The spectral resolution of the instrument was 0.45 nm/pixel for the grating with 300 groves/mm. For each source-detector pair 221 (every other point) of a maximum of 441 data pixels were acquired for the wavelength range 600 to 800 nm. This lower number of data pixels saved calculation time without significantly degrading the accuracy of the extracted quantities. The number of separation distances studied (typically 2 to 5 detection fibers) determined the final number of data points fit by the algorithm (*i.e.,* 442 to 1105 data points, respectively). The tissue sampling depth is approximately half of the source-detector separation distance, *i.e.,* ~0.6 to 2 mm for tumors in these studies.

Data inversion used an algorithm based on the diffusion equation with the constraint that $\mu_s' = A\lambda^{-B}$ and $\mu_a = \Sigma\, c_i\epsilon_i\,(\lambda)$. Here λ is the wavelength; A and B are related to the scatterer size, index of refraction, and concentration (24, 25); and c_i and ϵ_i are the concentration and extinction coefficient of the i^{th} chromophore, respectively. Primary tissue chromophores were oxyhemoglobin (HbO_2), deoxyhemoglobin (Hb), Photofrin, and water; the extinction coefficients of HbO_2, Hb, and water were obtained from the literature.[4] The extinction coefficient of Photofrin was measured by us using an absorption spectrometer (Ocean Optics, Dunedin, FL). The extinction coefficients of HbO_2 and Hb used in this study were comparable with those referenced in other studies (26, 27).

The diffuse reflectance algorithm simultaneously fit data from all wavelengths to well studied analytical solutions for semi-infinite turbid media (28–35), to extract A, B, $c_{Photofrin}$, c_{water}, c_{HbO2}, and c_{Hb}. From these quantities we calculated tumor physiologic parameters including total hemoglobin concentration (THC = $c_{HbO2} + c_{Hb}$), tissue hemoglobin oxygen saturation ($SO_2 = c_{HbO2}/THC$), $\mu_s'(\lambda) = A\lambda^{-B}$, $\mu_a(\lambda) = \Sigma\, c_i\epsilon_i\,(\lambda)$, and the effective attenuation coefficient μ_{eff} at the treatment wavelength of 630 nm. The effective attenuation coefficient μ_{eff} characterizes the exponential decrease of light as it penetrates tissue and is a function of the reduced scattering and absorption coefficients, defined as $\mu_{eff} = [3\,\mu_a(\mu_a + \mu_s')]^{1/2}$ from diffusion theory (23). The effective attenuation coefficient can be different for each tissue, and its inverse is defined as the light penetration depth $\delta\,(= 1/\mu_{eff})$, *i.e.,* the depth at which light entering tissue is reduced to ~37% or 1/e of its incident value (36).

Optical property measurements were collected before and immediately after PDT. In carbogen-breathing animals, measurements were taken before and after 15 minutes of carbogen breathing; when applicable, PDT was then performed under continued carbogen breathing. At each time point, ~10 to 20 measurements were taken over multiple tumor sites with an acquisition time of 100 ms/measurement. Approximately 2 seconds (700MHz Pentium III processor) were required to apply the global algorithm to data collected from each site (442 to 1105 data points, as described above).

In other studies, we verified the accuracy and defined the coefficient of variance of this system using blood-containing optical tissue phantoms (23). For example, in tissue-simulating phantoms diluted from 30% Liposyn III (Abbott Laboratories, Chicago, IL) in PBS to 1%, 1.5%, and 2% (corresponding $\mu_s' = 10$, 15, and 20 cm^{-1} at 830 nm, respectively). The measured μ_s' was found to have an accuracy of 106%, 105%, and 101% respectively. That is, the values of μ_s' were recovered to within 6% of their true values, and the coefficient of variance was <0.3% for all three of the Liposyn concentrations. In tissue-simulating phantoms containing human erythrocytes, μ_a typically had a similar accuracy (~105%) and coefficient of variance (<0.6%). Finally, SO_2 typically had a coefficient of variance of <1.5% in a single location and ~2% to 7% when averaged over the whole tumor.

Tissue Phantom Oxygenation. The SO_2 and pO_2 of a solution of mouse erythrocytes was measured over the course of its deoxygenation using broadband reflectance spectroscopy and the Eppendorf pO_2 histograph (or Clark-style microelectrodes; ref. 37), respectively. Blood drawn by cardiac puncture from C3H mice was collected in tubes containing sodium heparin, centrifuged, rinsed two to three times in PBS, and diluted to 90 μmol/L (hemoglobin concentration) in a solution of ~1% diluted Liposyn III (Abbott Laboratories) in PBS (31). This solution was gently stirred in a covered container (37°C) as nitrogen was bubbled in. The Clark-style miroelectrode and pO_2 histograph probe were both immersed in the phantom, whereas the spectrometer probe was fixed in position at the surface. Oxygen measurements by all three of the instruments were begun before adding N_2 and continued at regular intervals of ≤2 minutes during N_2 delivery. The Clark-style microelectrode and Eppendorf pO_2 histograph were precalibrated for the 37°C operating temperature, and the pO_2 histograph was precalibrated for the barometric pressure. A reference voltage for the pO_2 histograph was provided was by clamping the reference electrode to a copper wire immersed in the solution. The pO_2 histograph was operated in a stationary position by setting the measurement path, step length, and overstroke to 0 cm; it was calibrated in saline bubbled with air or nitrogen, as per the manufacturer's instructions. Studies were performed in duplicate.

***In vivo* Oxygenation Measured by Broadband Reflectance Spectroscopy *versus* the Eppendorf pO_2 Histograph.** Tumor SO_2 measurement by broadband reflectance spectroscopy was compared with tumor pO_2 measurement by the Eppendorf pO_2 histograph as the carbogen-induced change in SO_2 or pO_2. Tumors were studied at size of ~7 to 8 mm in diameter to facilitate placement of the spectrometer probe on tissue uninjured by the pO_2 histograph probe. This was additionally aided by minimizing the "stepping" motion of the pO_2 histograph probe. A single, manual pilgrim step was used to eliminate pressure artifacts at the probe tip, then data acquisition was begun. A total of ~20 data points were collected and postcalibrated for tissue temperature and barometric pressure. The probe was calibrated in saline bubbled with air or nitrogen, as per the manufacturer's instructions.

Precarbogen tumor oxygenation in anesthetized (isoflurane) animals was first measured by the Eppendorf pO_2 histograph. After precarbogen pO_2 measurement, the spectrometer probe was clamped in a fixed, virgin position on the tumor, and SO_2 data (20 measurements with 8,000 data points) were collected before and after 15 minutes of carbogen breathing. After SO_2 measurement during carbogen breathing, the spectrometer probe was removed and pO_2 during carbogen breathing was measured by the pO_2 histograph.

Statistics. For animals with tumors that recurred, the data for treatment durability and each parameter of interest [relative-SO_2, SO_2 after PDT

[4] S. Prahl, 2001. Optical properties spectra. Internet address: http://omlc.ogi.edu/spectra/index.html.

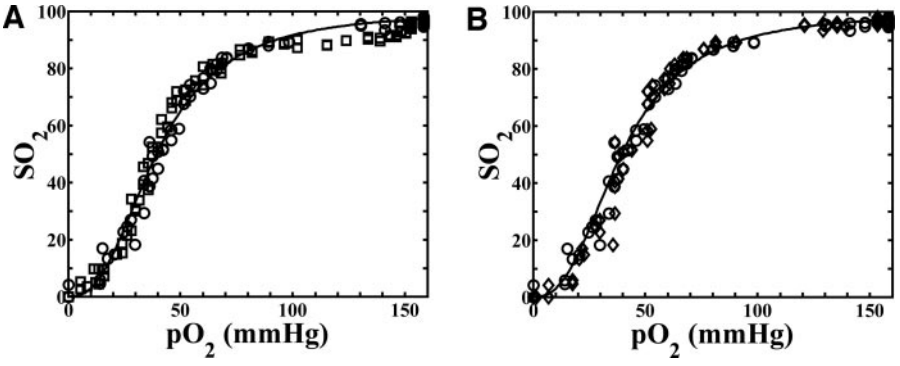

Fig. 1. *A*, the oxyhemoglobin dissociation curve for mouse erythrocytes in a tissue phantom. Over the course of phantom deoxygenation, SO_2 and pO_2 were simultaneously measured by broadband reflectance spectroscopy and the Eppendorf pO_2 histograph, respectively. Plots depict the results of two separate studies. Data were fit by the mathematical equation $SO_2 = pO_2^n/(p50^n + pO_2^n)$ yielding the estimates, p50 = 39.37 0.33, n = 2.558 0.056. *B*, the oxyhemoglobin dissociation curve based on pO_2 measurements by the Eppendorf pO_2 histograph (○) *versus* Clark-style electrodes (◇). SO_2 was measured by broadband reflectance spectroscopy. Plots demonstrate one of duplicate studies with each instrument.

($SO_{2\ after}$), SO_2 before PDT ($SO_{2\ before}$), and tumor volume or light penetration] were fit to a linear model. The strength of the association was assessed by the correlation coefficient (r^2) with statistical significance given by a Wald test comparing the estimated slope to a slope of 0. Relative-SO_2 *versus* relative-pO_2 or $SO_{2\ before}$ were also fit with a linear model and assessed by r^2 and the Wald test. The Wilcoxon rank sum was used to test for differences in the median level of the parameter of interest between groups; the Wilcoxon signed rank test was used to test for differences in the median level of the parameter of interest within groups, *e.g.*, if the median relative-SO_2 values were significantly different from a value of 1. Plots of Kaplan-Meier estimates of the survival (absence of recurrence) probabilities were used to describe the overall pattern of response in the data (38), where animal groups were defined based on whether their relative-SO_2 fell above or below the sample median. Statistical significance of the association between survival and relative-SO_2 or carbogen-breathing, along with 95% confidence intervals on the relative risk of failure, were based on univariate Cox proportional hazard models. Cox proportional hazards models were developed in R 1.7 (free software; ref. 39)[5]; all of the other tests were performed in JMP (SAS Institute, Inc.). For all tests a type I error rate of 0.05 was used with Ps < 0.05 considered statistically significant.

Relative-SO_2 was based on the ratio of the mean value for $SO_{2\ after}$ to $SO_{2\ before}$ in an individual animal. Each mean was calculated from a minimum of 5 repeated measurements in the same tumor (although the majority of tumors were sampled 20 times). We used a resampling technique to estimate the SE of the relative-SO_2 ratio for each animal. Briefly, the before and after data were resampled 1,000 times, forming the relative-SO_2 ratio for each sample. The SE was estimated from the resampled ratios (40). Two animals did not have a sufficient number of nonzero measurements to obtain a reliable estimate of the SE.

RESULTS

Broadband Reflectance Spectroscopy Measurement of Tissue Hemoglobin Oxygen Saturation. Reflectance diffuse spectroscopy measurement of tissue oxygenation is a well-established methodology (21, 32, 34, 41–44). In addition, validation of our diffuse optical reflectance approach in tissues has been reported in brain activation (33, 45) and tumor studies (46). To additionally evaluate the diffuse reflectance approach in the context of the present studies, we measured the SO_2 of a tissue phantom of mouse erythrocytes over the course of its deoxygenation. The oxygen partial pressure (pO_2) of the phantom was measured by the Eppendorf pO_2 histograph and Clark-style oxygen microelectrodes. Fig. 1*A* plots the oxyhemoglobin dissociation curve for mouse blood based on the spectroscopy-measured SO_2 values and the pO_2 histograph-measured pO_2 values. This curve closely matches that published by others (47). For example, at an SO_2 of 50% we found pO_2 to be 39.37 0.33 mm Hg compared with a value of ~40 mm Hg depicted in the curve published by Gray and Steadman (47). Curves based on pO_2 measured by the Eppendorf pO_2 histograph were in excellent agreement with those based on Clark-style electrode measurements (Fig. 1*B*).

In vivo validation of broadband reflectance spectroscopy was performed through comparison of the carbogen-induced change in radiation-induced fibrosarcoma tumor SO_2, measured by spectroscopy, *versus* the change in pO_2, measured by the Eppendorf pO_2 histograph. In each of 6 animals the relative change in SO_2 or pO_2 (relative-SO_2 or relative-pO_2) was calculated as the ratio of SO_2 or pO_2 after carbogen breathing to the precarbogen value in the same animal. Fig. 2 plots relative-SO_2 *versus* relative-pO_2. The correlation coefficient (r^2) of the data fit to the linear regression line is 0.90, and the slope of the line is significantly different from zero ($P = 0.0038$). Thus, good agreement between the relative-SO_2 and -pO_2 data were found.

In additional consideration of the ratios plotted in Fig. 2, we sought to account for the consequences of the nonlinear relationship between SO_2 and pO_2, which can affect the calculated ratios. To avoid the effects of this nonlinearity, pO_2 data were converted to SO_2 based on the oxyhemoglobin dissociation curve of Fig. 1*A*, and ratios were recalculated. The fit of the linear relationship (data not shown) between relative-SO_2 and relative-pO_2-based SO_2 was slightly poorer ($r^2 = 0.81$, $P = 0.015$) than that of relative-SO_2 *versus* relative-pO_2, yet still highly significant. Overall, the good agreement between relative oxygenation changes measured by the Eppendorf pO_2 histograph and our broadband reflectance spectrometer provides strong *in vivo* validation of our system.

Tumor Optical and Physiologic Properties. Table 1 summarizes the physiologic and optical properties of radiation-induced fibrosarcoma tumors treated with Photofrin-PDT at 38 mW/cm^2, 135 J/cm^2,

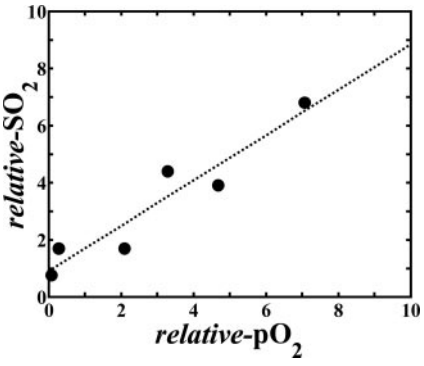

Fig. 2. In six radiation-induced fibrosarcoma tumors the carbogen-induced change in SO_2 *versus* the change in pO_2 is plotted, where SO_2 was measured by broadband reflectance spectroscopy and pO_2 by the Eppendorf pO_2 histograph. Relative-SO_2 or pO_2 was calculated by normalizing SO_2 or pO_2 after carbogen breathing to the precarbogen value in the same tumor. The correlation coefficient (r^2) of the data fit to the linear regression line is 0.90, and the slope is significantly different from a value of 0 ($P = 0.0038$). The SE in relative-SO_2 ranged from 0.002 to 0.16 (median = 0.023) among mice.

[5] Internet address: http://www.r-project.org.

and control (light-treated) animals. At the time of illumination all of the tumors had volumes of <100 mm^3, with a median tumor size of 42.26 mm^3 and 46.20 mm^3 in the control and treated animals, respectively. Median time-of-tumor-growth to the end point of a 400-mm^3 tumor volume was 7 days in controls and 18 days in PDT-treated animals. No statistical association between initial tumor volume and time-to-400 mm^3 was found in either the control or treated animals ($r^2 = 0.39$ and 0.18, $P = 0.09$ and 0.17, respectively). Tumor optical properties before illumination, namely the reduced scattering coefficient (μ_s') and absorption coefficient (μ_a), at the treatment wavelength of 630 nm were consistent between groups. Consequently, similar median light penetration (δ) was detected in the control and PDT-treated groups. Light penetration was also very similar among the PDT-treated mice (range, 0.21 to 0.34 cm), and, in animals that recurred, no association between δ and tumor time-to-400 mm^3 was found ($r^2 = 0.24$, $P = 0.10$). This suggests that response to PDT was not significantly affected by small tumor-to-tumor variations in attenuation of treatment light. No effect of PDT on tumor optical properties was found (data not shown).

SO_2 before light administration was similar between control and PDT-treated tumors, with median values of 28.43% and 27.84%, respectively (Table 1). Immediately after delivery of 630 nm illumination (135 J/cm^2 and 38 mW/cm^2), median SO_2 was 22.25% and 29.86% in the control and photosensitized tumors, respectively, with no significant difference detected between groups. In contrast, the light-induced change in SO_2 (relative-SO_2) was higher ($P = 0.022$) in PDT-treated (1.45) than in control animals (0.85). The relative-SO_2 in the control group was not significantly different from a value of 1 ($P = 0.15$), whereas in PDT-treated tumors the relative-SO_2 was significantly higher than 1 ($P = 0.034$). Therefore, most of the PDT-treated tumors exhibited increases in SO_2 immediately after illumination. However, response was variable, with relative-SO_2 ranging from 0.58 to 4.99 among PDT-treated tumors. We next investigated whether this variability in oxygenation responses to PDT was reflected in the long-term response of the tumors to treatment.

Photodynamic Therapy-Induced Change in Tumor SO_2 Is Highly Correlated with Response Durability. For animals that recurred, the association between the PDT-induced change in oxygenation, quantified as relative-SO_2, and treatment durability, measured by the time of tumor regrowth to 400 mm^3, is plotted in Fig. 3. Relative-SO_2 and tumor time-to-400 mm^3 were highly correlated ($r^2 = 0.80$), and the Wald test for a slope different from 0 was highly significant ($P < 0.0001$). The positive sign of the linear fit indicates improving PDT response with higher relative-SO_2: as expected, the larger the relative increase in oxygenation immediately after PDT, the more efficacious the tumor response.

Table 1 *Optical and physiological properties of PDT-treated radiation-induced fibrosarcoma tumors*

	Controls*		PDT-treated†	
	Median‡	Range‡	Median‡	Range‡
Time-to-400 mm^3 (percentage of cures)§	7 (0%)	3–10	18 (14%)	11–23
Pre- PDT tumor volume (mm^3)	42.26	28.16–80.49	46.20	27.71–70.54
μ_s' (cm^{-1}) at 630 nm	10.48	8.80–14.36	9.18	4.55–15.46
μ_a (cm^{-1}) at 630 nm	0.48	0.26–1.37	0.51	0.36–0.74
δ (cm) at 630 nm	0.25	0.16–0.38	0.27	0.21–0.34
SO_2 before light (%)	28.43	14.26–48.28	27.84	3.02–47.84
SO_2 after light (%)	22.25	11.95–49.59	29.86	9.94–48.94
Relative-SO_2¶	0.85	0.70–1.20	1.45	0.58–4.99

* Controls ($n = 8$) received illumination but no Photofrin.

† PDT-treated animals ($n = 14$) received Photofrin (5 mg/kg, 24 hour) and 630 nm illumination to 135 J/cm^2 at 38 mW/cm^2.

‡ Median and range given for all animals, including those that regrew and those that were cured.

§ Time-to-400 mm^3 indicates the day after control or PDT treatment that tumors reached a volume of 400 mm^3. The percentage of tumor-free (cured) animals at 90 days after PDT is indicated in parentheses.

¶ Relative-SO_2 was calculated as the ratio of SO_2 after light delivery to the pre-light value.

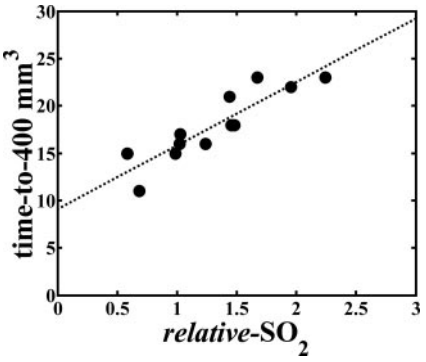

Fig. 3. The association between treatment durability and the PDT-induced change in radiation-induced fibrosarcoma tumor oxygenation ($n = 12$). The day of tumor growth to a volume of 400 mm^3 (time-to-400 mm^3) is plotted as a function of the relative-SO_2, calculated as the SO_2 after PDT normalized to the pre-PDT value in the same tumor. The correlation coefficient (r^2) of the data fit to the linear regression line is 0.80, and the slope is significantly different from a value of 0 ($P < 0.0001$). Photofrin-sensitized mice with tumors <100 mm^3 received 630 nm illumination to 135 J/cm^2 at 38 mW/cm^2. The SE in relative-SO_2 ranged from 0.0007 to 0.029 (median = 0.006) among mice.

The Carbogen-Enhanced, Photodynamic Therapy-Induced Change in SO_2 Is Highly Correlated with Response Durability. The predictive value of spectroscopy-based SO_2 measurement in PDT was additionally validated in a separate group of animals under different oxygenation conditions. Animals were exposed to carbogen breathing for 15 minutes before PDT to increase the oxygenation of their tumors; PDT was then carried out using identical treatment conditions as above. Table 2 summarizes the optical and physiologic characteristics of tumors treated with carbogen and PDT. All of the tumors had volumes ≤100 mm^3, and no effect of volume on tumor time-to-400 mm^3 was detected in control or PDT-treated animals. No effect of carbogen breathing on tumor time-to-400 mm^3 was found in controls (compare a median regrowth time of 7 days in Table 1 *versus* 4 days in Table 2). The addition of carbogen breathing in PDT-treated animals increased the median time-to-400 mm^3 from 18 to 21 days and increased the percentage of cures from 14% to 30%, but these improvements failed to achieve statistical significance ($P = 0.34$). Tumor optical properties before carbogen breathing, including the light penetration depth, were similar between control and treated groups and among animals within each group.

Although carbogen breathing failed to significantly impact the average tumor response, it did result in significant increases in tumor oxygenation. After 15 minutes of carbogen breathing, median SO_2 increased from 36.45% to 63.95% ($P = 0.016$) in the controls and from 23.05% to 33.56% ($P = 0.002$) in the PDT-treated group (before PDT being performed). The addition of PDT resulted in additional increases in tumor oxygenation in this group of animals. The median relative-SO_2, calculated as the ratio of SO_2 after light delivery to the prelight (postcarbogen) value in the same animal, was 1.05 in controls and 1.65 in PDT-treated animals; only the latter was significantly different ($P = 0.01$) from a value of 1. Fig. 4 plots tumor time-to-400 mm^3 *versus* relative-SO_2 in mice exposed to carbogen breathing during PDT. Among these animals that recurred, treatment durability was highly correlated ($r^2 = 0.76$) with relative-SO_2, and the slope was significantly different from 0 ($P = 0.01$). Furthermore, the linear regression model fit to these data (time-to-400 $mm^3 = 12.4 + 4.33 \times$ relative-SO_2) was very similar to the model fit to mice treated with PDT in the absence of carbogen breathing (Fig. 3; time-to-400 $mm^3 = 9.09 + 6.7 \times$ relative-SO_2). The slopes (95% confidence interval)

Table 2 *Optical and physiologic properties of PDT-treated RIF tumors in carbogen-breathing animals*

	Controls*		PDT-treated†	
	Median‡	Range‡	Median‡	Range‡
Time-to-400 mm^3 (percentage of cures)§	4 (0%)	3–4	21 (30%)	14–22
Pre-PDT tumor volume (mm^3)	76.94	44.01–100.00	45.33	26.20–79.06
μ_s' (cm^{-1}) at 630 nm	10.77	6.14–14.93	10.18	8.29–19.30
μ_a (cm^{-1}) at 630 nm	0.66	0.41–0.90	0.54	0.38–0.95
δ (cm) at 630 nm	0.22	0.18–0.29	0.24	0.20–0.27
SO_2 before carbogen (%)	36.45	23.54–49.86	23.05	8.12–28.38
SO_2 after carbogen (before light) (%)	63.95	48.29–76.78	33.56	24.46–63.78
SO_2 after light (%)	64.92	54.33–74.01	64.62	30.93–77.76
Relative-SO_2¶	1.05	0.95–1.12	1.65	0.48–2.89

* Unphotosensitized controls ($n = 7$) began carbogen breathing 15 minutes before illumination.

† Photosensitized (Photofrin, 5 mg/kg, 24 hours), PDT-treated animals ($n = 10$) began carbogen breathing 15 minutes before illumination to 135 J/cm^2 at 38 mW/cm^2.

‡ Median and range given for all animals, including those that regrew and those that were cured.

§ Time-to-400 mm^3 indicates the day after control or PDT that tumors reached a volume of 400 mm^3. The percentage of tumor-free (cured) animals at 90 days after PDT is indicated in parentheses.

¶ Relative-SO_2 was calculated as the ratio of SO_2 after light delivery to the pre-light (after carbogen) value.

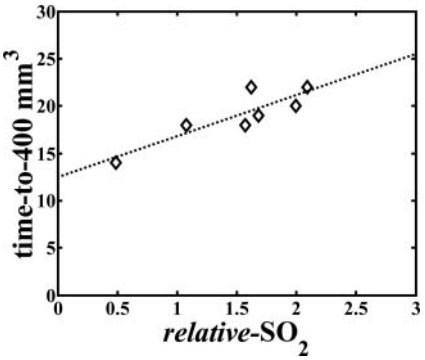

Fig. 4. The association between treatment durability and the PDT-induced change in radiation-induced fibrosarcoma tumor oxygenation ($n = 7$) in mice exposed to carbogen-breathing during PDT. Carbogen exposure was begun 15 minutes before PDT and continued throughout illumination. The day of tumor growth to a volume of 400 mm^3 (time-to-400 mm^3) is plotted as a function of the relative-SO_2, calculated as the SO_2 after PDT normalized to the pre-PDT (after carbogen) value in the same tumor. The correlation coefficient (r^2) of the data fit to the linear regression line is 0.76, and the slope is significantly different from a value of 0 ($P = 0.01$). Photofrin-sensitized mice with tumors <100 mm^3 received 630 nm illumination to 135 J/cm^2 at 38 mW/cm^2. The SE in relative-SO_2 ranged from 0.001 to 0.008 (median = 0.005) among mice.

of the models (4.33 2.80 and 6.7 2.31) demonstrate substantial overlap. In fact, all of the PDT-treated mice that recurred, both air and carbogen-breathing, can be well fit with a single model: time-to-400 $mm^3 = 10.37 + 5.74 \times$ relative-SO_2 ($r^2 = 0.77$, $P < 0.0001$; see Fig. 5).

In carbogen-breathing animals, the relative-SO_2 can also be calculated based on the SO_2 before carbogen breathing instead of the SO_2 immediately before PDT (after carbogen breathing). In this case values of relative-SO_2 are higher (range, 1.09 to 6.3), because they reflect increases in tumor oxygenation from both carbogen breathing and PDT. For animals that recurred, the association between PDT-induced change in SO_2 and treatment durability remains significant ($r^2 = 0.72$, $P = 0.02$) when relative-SO_2 is based on the precarbogen value (data not shown).

Photodynamic Therapy-Induced Change in Tumor SO_2 Is Predictive of Survival Time. In both air- and carbogen-breathing animals PDT was successful in creating some tumor cures. Fig. 5 summarizes relative-SO_2 values in all of the PDT-treated animals, including both those that recurred and those that were cured. As is visible in this figure, cured animals trended toward higher relative-SO_2 values. Cox proportional hazards models of animal survival were used to include cured animals in analyses, where survival was defined as maintenance of a tumor volume <400 mm^3. In practice, all of the survivors, *i.e.*, cured animals, demonstrated no sign of tumor recurrence. Conversely, failure was the event whereby a tumor obtained a volume ≥ 400 mm^3. In air-breathing animals, increasing relative-SO_2 was significantly associated ($P = 0.0013$) with better survival time. In carbogen-breathing animals, the association between increasing relative-SO_2 and better survival approached but did not reach statistical significance ($P = 0.057$). The confidence intervals on the risk of failure demonstrated a large degree of overlap between these two groups, so we also considered the results for both groups of animals together. In all of the animals, both air- and carbogen-breathing, a highly significant association ($P = 0.00011$) was found between increasing relative-SO_2 and survival time. The model including all of the animals predicts that those with a relative-SO_2 of 2 had a 7% (95% confidence interval of 2% to 27%) risk of failure compared with those with no change in SO_2 after PDT (relative-$SO_2 = 1$). Kaplan-Meier curves (Fig. 6) of animal response, segregated by median relative SO_2 value, demonstrate a longer median regrowth time (22.5 *versus* 16.5 days) and greater number of cures (33% *versus* 8%) in animals with "high" (above the median) relative-SO_2 compared with animals with "low" (below the median) relative-SO_2.

SO_2 Immediately Before or After Photodynamic Therapy Is Poorly Associated with Tumor Response. Absolute tumor oxygenation before or after PDT was also evaluated as possible predictors of tumor response. SO_2 immediately before PDT ($SO_{2\ \text{before}}$) varied widely in animals cured by PDT, *i.e.*, those with no tumor recurrence at 90 days after treatment (Fig. 7). However, for animals that recurred, treatment durability was weakly ($r^2 = 0.45$, 0.52, and 0.29 for air-breathing, carbogen-breathing, and all mice, respectively), but, in general, significantly ($P = 0.017$, 0.064, and 0.017, respectively) associated with $SO_{2\ \text{before}}$. Surprisingly, the direction of this association was negative, *i.e.*, tumors with lower $SO_{2\ \text{before}}$ demonstrated longer time-to-400 mm^3. An explanation for this unexpected finding is evident in Fig. 8; namely, tumors with lower SO_2 before had larger relative increases in SO_2 after PDT ($r^2 = 0.56$, $P = 0.0001$). SO_2 immediately after PDT ($SO_{2\ \text{after}}$) also varied substantially among cured animals (Fig. 9). No association ($r^2 = 0.08$, 0.44, and 0.17; $P = 0.38$, 0.11, and 0.08, in air-breathing, carbogen-breathing, and all mice, respectively) was detected between $SO_{2\ \text{after}}$ and treatment durability.

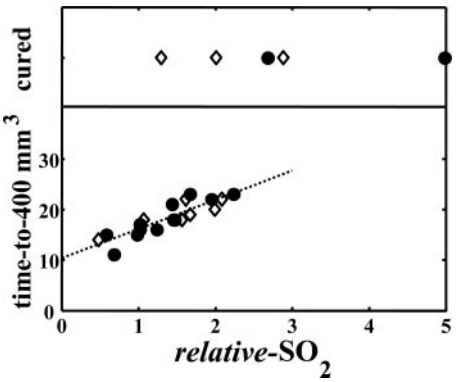

Fig. 5. A summary of relative-SO_2 values in all PDT-treated mice ($n = 24$), air- (●) and carbogen-breathing (◇), including those that recurred (*bottom*) and those cured (*top*) by PDT. A linear regression model fit to mice that recurred ($n = 19$) predicts that enhanced treatment durability (time-to-400 mm^3) is significantly associated with higher relative-SO_2 ($r^2 = 0.77$, $P < 0.0001$). Please refer to the legends of Figs. 3 and 4 for a definition of relative-SO_2 in the air and carbogen-breathing animals, respectively. The SE in relative-SO_2 ranged from 0.0007 to 0.27 (median = 0.007) among all mice ($n = 24$).

DISCUSSION

The oxygen dependence of PDT is well studied, with numerous reports of more durable tumor response in animal groups receiving oxygen-sparing PDT (3, 4, 48). However, in PDT few have studied the predictive value of tumor oxygenation at the level of individual tumors. In one report, Pham *et al.* (21) found that PDT-created decreases in tumor SO_2 were highly correlated with tumor area of necrosis. Such studies ideally require a rapid, noninvasive method of measuring average tumor oxygen concentration. We have used broadband reflectance spectroscopy to perform such an investigation, finding that knowledge of changes in the oxygenation of a tumor within minutes after PDT can be used to predict its long-term treatment response.

Reflectance diffuse spectroscopy is a well-documented technique of measuring tissue optical properties, including concentrations of oxyhemoglobin and deoxyhemoglobin (21, 32, 34, 35, 41–44). From these quantities tissue hemoglobin oxygen saturation, or SO_2, can be calculated. Our custom, handheld spectrometer probe facilitated rapid, noninvasive measurement of optical properties at multiple tumor sites. Each measurement provided data on tumor oxygenation at depths up to one half of the maximum utilizable source-detector separation distance, *i.e.*, typically depths of 0.6 to 2.0 mm. Mouse skin is only ~0.25-mm thick (49), whereas tumors were ~2 to 3 mm in thickness; accordingly, tumor was the major tissue type contributing to the detected signal. Manual movement of the probe to ~10 to 20 unique positions on each tumor ensured that measured properties were spatially averaged.

The data show a strong positive correlation between the normalized PDT-created change in tumor oxygenation (relative-SO_2) and treatment durability. The positive sign of the correlation between relative-SO_2 and time-to-400 mm^3 indicates that better responses are associated with a larger relative increase (or conversely, a smaller decrease) in tumor oxygenation. Furthermore, higher relative-SO_2 values were significantly associated with better probability of survival, measured as the likelihood of a maintaining tumor volume <400 mm^3, *i.e.*, absence of recurrence. Investigations were conducted in two separate groups of animals: air-breathing animals with unaltered pre-PDT tumor oxygenation and carbogen-breathing animals with enhanced SO_2. In the case of carbogen-induced increases in pre-PDT tumor oxygenation, PDT-induced change in SO_2 was still predictive of tumor response. Furthermore, linear regression models fit to the air-breathing and carbogen-breathing animals were similar, and all of

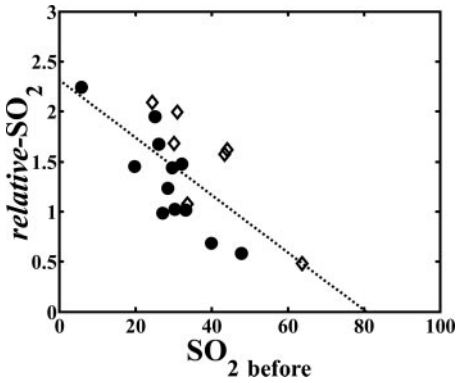

Fig. 8. The association between relative-SO_2 and tumor oxygenation before PDT ($SO_{2\ before}$) in PDT-treated animals analyzed for durability of response ($n = 19$). Relative-SO_2 was calculated as the ratio of SO_2 after PDT normalized to SO_2 before PDT (after carbogen in carbogen-breathing animals). The correlation coefficient (r^2) of the data fit to the linear regression line is 0.56, and the slope is significantly different from a value of 0 ($P = 0.0001$). The SE in relative-SO_2 ranged from 0.0007 to 0.029 (median = 0.006) among mice.

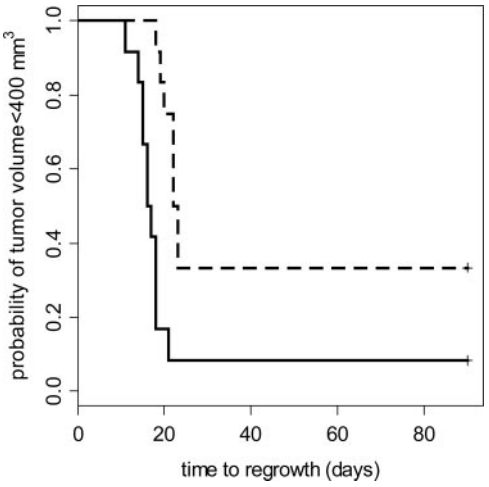

Fig. 6. Kaplan-Meier curves of animal survival, *i.e.*, a tumor volume <400 mm^3, after Photofrin-PDT with 630-nm illumination to 135 J/cm^2 at 38 mW/cm^2. Animals (air- and carbogen-breathing; $n = 24$) were segregated based on relative-SO_2 value into those with "high" relative-SO_2 (*dashed line*), greater than the sample median, and those with "low" relative-SO_2 (*solid line*), below the median. Animals with "high" relative-SO_2 demonstrate a longer median regrowth time (22.5 *versus* 16.5 days) and a greater number of cures (33% *versus* 8%) than animals with "low" relative-SO_2. Cox proportional hazards models detect a significant association ($P = 0.00011$) between increasing relative-SO_2 and improving survival.

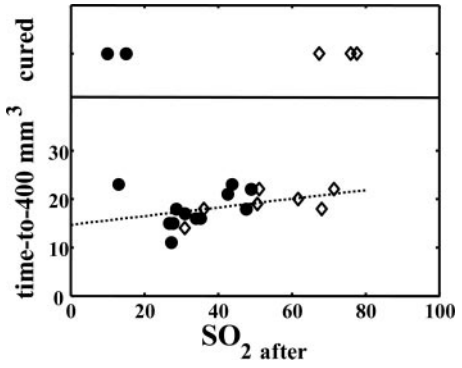

Fig. 9. A summary of SO_2 values after PDT ($SO_{2\ after}$) in all treated mice ($n = 24$), air- (●) and carbogen-breathing (◇), including those that recurred (*bottom*) and those cured (*top*) by PDT. Among mice that recurred ($n = 19$), no association ($r^2 = 0.17$, $P = 0.08$) between treatment durability (time-to-400 mm^3) and $SO_{2\ after}$ was detectable. The SE in SO_2 after ranged from 2.3 to 17.0 (median = 10.9) among all mice ($n = 24$).

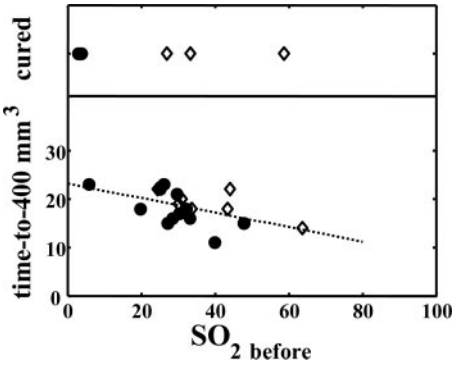

Fig. 7. A summary of SO_2 values before PDT ($SO_{2\ before}$) in all treated mice ($n = 24$), air- (●) and carbogen-breathing (◇), including those that recurred (*bottom*) and those cured (*top*) by PDT. A linear regression model fit to mice that recurred ($n = 19$) predicts that enhanced treatment durability (time-to-400 mm^3) is weakly but significantly associated with lower $SO_{2\ before}$ ($r^2 = 0.29$, $P = 0.017$). The SE in $SO_{2\ before}$ ranged from 0.7 to 23.7 (median = 8.0) among all mice ($n = 24$).

the animals, both air- and carbogen-breathing, could very accurately be fit with a single model. This finding suggests that the relative-SO_2 is a useful marker of the PDT tumor response. Continuing studies with other PDT photosensitizers/illumination protocols and in other tumor models will additionally test its application.

The predictive value of relative-SO_2 likely relates to its direct reporting of an effector or process immediately relevant to PDT tumor response. Increases in tumor oxygenation during or after PDT, especially to values greater than the pre-PDT level, may be a result of PDT-induced increases in blood flow (8). In our studies, small increases in tumor temperature (~3°C) were detected over the course of illumination. However, tumor concentrations of hemoglobin tended to increase after PDT, rising from a median of 120 to 143 μmol/L in air-breathing mice ($P = 0.058$) and from 123 to 176 μmol/L in carbogen-breathing mice ($P = 0.020$), suggesting that many mice experienced small increases in tumor blood flow in the minutes after illumination. Others have suggested that enhanced tumor oxygenation after PDT may be associated with decreases in cellular metabolism due to cell kill (7, 13).

Compared with relative-SO_2, as an independent variable the SO_2 before PDT was poorly associated with treatment response. The tumors of this study were generally well oxygenated, with all of the tumors exhibiting a pre-PDT SO_2 3.02%, corresponding to a pO_2 of 10.15 mm Hg: well above the half-value (7.6 mm Hg) for PDT inactivation of tumor cells (50). Others have also found that low levels of pre-PDT tumor hypoxia do not limit therapy response (51). The trend between decreasing SO_2 and better treatment durability can be explained by the negative association between SO_2 immediately before PDT and relative-SO_2. In rats exposed to carbogen, Hull *et al.* (41) reported a correlation between decreasing baseline oxygenation and increasing carbogen-induced enhancement of tumor SO_2. In the present study, we found a similar pattern ($r^2 = 0.33$, $P = 0.02$) between decreasing precarbogen SO_2 and increasing magnitude of the carbogen-induced relative change in SO_2 (data not shown). One interpretation of these data is based on the shape of the oxyhemoglobin dissociation curve (41). The characteristic shape of this curve predicts a steep linear association between SO_2 and pO_2 at SO_2 values <80%, followed by a flattening of the curve at 80% SO_2 such that large increases in pO_2 create very small increases in SO_2. In the tumors of the present study, absolute SO_2 never exceeded 80% (see Tables 1 and 2) and, thus, remained on the linear portion of the curve. Taken together these data suggest that tumors with moderate oxygenation can demonstrate large increases in SO_2 in response to PDT (or carbogen breathing).

As an independent parameter, the SO_2 immediately after PDT was not predictive of treatment durability or survival, although the trend was toward increasing SO_2 in animals with better PDT response. This finding additionally emphasizes the need for monitoring of PDT-induced changes in tumor oxygenation, as opposed to measuring SO_2 at single time points immediately surrounding illumination.

Measured values for tumor SO_2 before and after PDT were highly variable, ranging from 3% to 48% before PDT and from 10% to 49% immediately after PDT in air-breathing animals, although such variability is in good agreement with that reported by some others. Pogue *et al.* (6) measured pO_2 to vary from <1 to ~20 mmHg in a rat mammary carcinoma both before and during PDT. Henderson *et al.* (8) reported that the pO_2 of human basal cell carcinomas varied from 2.7 to 52.4 mm Hg before PDT and from 0 to 55.2 mm Hg during treatment. Using cryospectrophotometric techniques, Rofstad *et al.* (52) measured tumor intravascular HbO_2 saturations to range from 0% to 90% in radiation-induced fibrosarcoma tumors. The median intravascular HbO_2 saturation was between 20% and 30% for all of the blood vessels measured. This value agrees very well with our intertumoral SO_2 median of ~23% to 36%, although notably our measurements are not capable of determining the HbO_2 saturation within single vessels. No association between tumor SO_2 and tumor volume (data not shown) was detected in this study.

Reflectance spectroscopy is a well-established methodology in studies of tissue optics and physiology; however, its application in the PDT field has been limited. A more commonly used method for studying the oxygenation of PDT-treated tumors has been the Eppendorf pO_2 histograph (4, 8). We have provided validation of the broadband reflectance spectrometer through comparison of its measurements to those reported by the Eppendorf pO_2 histograph. *In vitro* studies accurately recreated the oxyhemoglobin dissociation curve for mouse blood based on absolute measurement of SO_2 (broadband reflectance spectroscopy) and pO_2 (Eppendorf pO_2 histograph). Independent pO_2 measurement with a Clark-style microelectrode confirmed that detected by the Eppendorf pO_2 histograph. *In vivo* studies were designed to measure the carbogen-induced change in tissue SO_2 and pO_2 with the broadband reflectance spectrometer and Eppendorf pO_2 histograph, respectively. The relative change in oxygenation, rather than absolute oxygenation values, was compared between instruments because the spectrometer and pO_2 histograph measure two different parameters, *i.e.*, SO_2 *versus* pO_2, and the use of relative values normalizes for systemic instrument-introduced variability in measurements, which may be different between the two instruments. The data show excellent correlation between the carbogen-induced change in tumor SO_2 and pO_2, providing *in vivo* validation of spectrometer-based measurement of SO_2 in this tumor model.

In addition to SO_2, tumor optical properties, including μ_s', μ_a, and δ, were measured. Generally, optical properties varied substantially less among tumors than did SO_2, and no association between optical properties and tumor response was detectable. In particular, the penetration depth of the treatment light (δ) exhibited limited tumor-to-tumor variation, ranging from 0.21 to 0.34 cm in air-breathing animals that went on to receive PDT. These values agree well with typical values of the penetration depth of 630 nm illumination, ranging from 1 to 3 mm for nonpigmented tissues (36).

The concentrations of Photofrin and water were also extracted outputs in the fitting process to the measured broadband reflectance spectrum. However, compared with the absorption coefficients of HbO_2 and Hb in tissue in the spectral range of 600 to 800 nm, the absorption coefficients of Photofrin and water are relatively small at 600 to 700 nm and are comparable with water at 750 to 800 nm. As an example, for tissue having 100 μmol/L THC, 50% HbO_2, 10 μmol/L Photofrin, and maximal 100% (~55 mol/L) water, the absorption coefficient is 0.16, 0.73, 0.05, and 0.002 cm^{-1} at 600 nm for HbO_2, Hb, Photofrin, and water, respectively. At 750 nm, μ_a is 0.026, 0.70, 0.0, and 0.026 cm^{-1} for HbO_2, Hb, Photofrin, and water, respectively. Thus, the concentrations of HbO_2 and Hb are quite insensitive to the extracted quantities for Photofrin and water. Studies have reported water concentration in tissue using near-infrared spectroscopy in the spectral range of 700 to 1100 nm (21, 34, 53). Photofrin concentration is easily extracted using fluorescence techniques (54), which are of interest, but not used in this study.

The development of noninvasive means of implicit or explicit treatment dosimetry in PDT has expanded in recent years with reports on singlet oxygen monitoring (55), NADH fluorescence monitoring (56), ^{31}P magnetic resonance spectroscopy (57, 58), and BOLD-contrast magnetic resonance imaging (59) providing evidence of potential utilization of each technique in PDT. Broadband reflectance spectroscopy is based on the diffusion model and photon migration inside scattering media, similar to near-infrared

photon-migration spectroscopy reported by Pham *et al.* (21). The advantages of broadband reflectance spectroscopy among near-infrared and many other spectroscopy techniques are the rapid data acquisition time, the relative low cost of the needed equipment, and the simple instrumentation. In conclusion, this study demonstrates that a broadband continuous wave reflectance spectroscopy system can be used noninvasively to rapidly extract information on tissue optical properties and tissue hemoglobin oxygen saturation (SO_2) before and after PDT. We have shown that PDT-induced changes in tumor oxygenation, as measured by this method, highly correlate with tumor response in an animal model. Continuing studies will evaluate the value of oxygen monitoring as a universal tool in oncological applications of PDT.

ACKNOWLEDGMENTS

We acknowledge technical assistance by Vanessa Madrak and helpful conversations with Drs. Steve M. Hahn, Timothy C. Zhu, Turgut Durduran, Guoqiang Yu, and Jarod Finlay. We thank Dr. Cameron J. Koch for use of the Clark-style electrode probe and Drs. Koch and Finlay for assistance with the tissue phantom experiments.

REFERENCES

1. Dougherty TJ, Gomer CJ, Henderson BW, et al. Photodynamic therapy. J Natl Cancer Inst 1998;90:889–905.
2. Tromberg BJ, Orenstein A, Kimel S, et al. In vivo tumor oxygen tension measurements for the evaluation of the efficiency of photodynamic therapy. Photochem Photobiol 1990;52:375–85.
3. Foster TH, Murant RS, Bryant RG, et al. Oxygen consumption and diffusion effects in photodynamic therapy. Radiat Res 1991;126:296–303.
4. Sitnik TM, Hampton JA, Henderson BW. Reduction of tumour oxygenation during and after photodynamic therapy in vivo: effects of fluence rate. Br J Cancer 1998; 77:1386–94.
5. Zilberstein J, Bromberg A, Frantz A, et al. Light-dependent oxygen consumption in bacteriochlorophyll-serine-treated melanoma tumors: on-line determination using a tissue-inserted oxygen microsensor. Photochem Photobiol 1997;65:1012–9.
6. Pogue BW, Braun RD, Lanzen JL, Erickson C, Dewhirst MW. Analysis of the heterogeneity of pO2 dynamics during photodynamic therapy with verteporfin. Photochem Photobiol 2001;74:700–6.
7. Pogue BW, O'Hara JA, Goodwin IA, et al. Tumor pO2 changes during photodynamic therapy depend upon photosensitizer type and time after injection. Comparative Biochemistry and Physiology Part A 2002;132:177–84.
8. Henderson BW, Busch TM, Vaughan LA, et al. Photofrin photodynamic therapy can significantly deplete or preserve oxygenation in human basal cell carcinomas during treatment, depending on fluence rate. Cancer Res 2000;60:525–9.
9. Sitnik TM, Henderson BW. The effect of fluence rate on tumor and normal tissue responses to photodynamic therapy. Photochem Photobiol 1998;67:462–6.
10. van Geel IP, Oppelaar H, Marijnissen JP, Stewart FA. Influence of fractionation and fluence rate in photodynamic therapy with Photofrin or mTHPC. Radiat Res 1996; 145:602–9.
11. Gibson SL, Foster TH, Feins RH, et al. Effects of photodynamic therapy on xenografts of human mesothelioma and rat mammary carcinoma in nude mice. Br J Cancer 1994;69:473–81.
12. Curnow A, Haller JC, Bown SG. Oxygen monitoring during 5-aminolaevulinic acid induced photodynamic therapy in normal rat colon. Comparison of continuous and fractionated light regimes. J Photochem Photobiol B 2000;58:149–55.
13. Pogue BW, O'Hara JA, Demidenki E, et al. Photodynamic therapy with verteporfin in the radiation-induced fibrosarcoma-1 tumor causes enhanced radiation sensitivity. Cancer Res 2003;63:1025–33.
14. Busch TM, Wileyto EP, Emanuele MJ, et al. Photodynamic therapy creates fluence rate-dependent gradients in the intratumoral spatial distribution of oxygen. Cancer Res 2002;62:7273–9.
15. Busch TM, Hahn SM, Evans SM, Koch CJ. Depletion of tumor oxygenation during photodynamic therapy: detection by the hypoxia marker EF3 [2-(2-Nitroimidazol-1[H]-yl)-N-(3,3,3-trifluoropropyl)acetamide]. Cancer Res 2000;60:2636–42.
16. van Geel IP, Oppelaar H, Rijken PF, et al. Vascular perfusion and hypoxic areas in RIF-1 tumours after photodynamic therapy. Br J Cancer 1996;73:288–93.
17. Moore RB, Chapman JD, Mercer JR, et al. Measurement of PDT-induced hypoxia in dunning prostate tumors by iodine-123-iodoazomycin arabinoside. J Nucl Med 1993; 34:405–11.
18. Schouwink H, Oppelaar H, Ruevekamp M, et al. Oxygen depletion during and after mTHPC-mediated photodynamic therapy in RIF1 and H-MESO1 tumors. Radiat Res 2003;159:190–8.
19. Chapman JD, McPhee MS, Walz N, et al. Nuclear magnetic resonance spectroscopy and sensitizer-adduct measurements of photodynamic therapy-induced ischemia in solid tumors. J Natl Cancer Inst 1991;83:1650–9.
20. McIlroy BW, Curnow A, Buonaccorsi G, et al. Spatial measurement of oxygen levels during photodynamic therapy using time-resolved optical spectroscopy. J Photochem Photobiol B 1998;43:47–55.
21. Pham TH, Hornung R, Berns MW, Tadir Y, Tromberg BJ. Monitoring tumor response during photodynamic therapy using near-infrared photon-migration spectroscopy. Photochem Photobiol 2001;73:669–77.
22. Solonenko M, Cheung R, Busch TM, et al. In vivo reflectance measurement of optical properties, blood oxygenation and motexafin lutetium uptake in canine large bowels, kidneys, and prostates. Phys Med Biol 2002;47:857–73.
23. Wang H-W, Zhu TC, Putt ME, et al. Broadband reflectance measurements of light penetration, blood oxygenation, hemoglobin concentration, and drug concentration in human intraperitoneal tissues before and after photodynamic therapy. J Biomedical Optics. In press 2004.
24. Bevilacqua F, Berger AJ, Cerussi D, Jakubowski D, Tromberg BJ. Broadband absorption spectroscopy in turbid media by combined frequency-domain and steady-state methods. Appl Opt 2000;39:6498–507.
25. Mourant JR, Fuselier T, Boyer J, Johnson TM, Bigio IJ. Predictions and measurements of scattering and absorption over broad wavelength ranges in tissue phantoms. Appl Opt 1997;36:949–57.
26. Zijlstra WG, Buursma A, Meeuwsen-van der Roest WP. Absorption spectra of human fetal and adult oxyhemoglobin, de-oxyhemoglobin, carboxyhemoglobin, and methemoglobin. Clin Chem 1991;37:1633–8.
27. Wray S, Cope M, Delpy DT, Wyatt JS, Reynolds EO. Characterization of the near infrared absorption spectra of cytochrome aa3 and haemoglobin for the non-invasive monitoring of cerebral oxygenation. Biochem Biophys Acta 1988;933:184–92.
28. Haskell RC, Svaasand LO, Tsay T-T, et al. Boundary conditions for the diffusion equation in radiative transfer. J Opt Soc Am A 1994;11: 2727–41.
29. Kienle A, Patterson MS. Improved solutions of the steady-state and the time-resolved diffusion equations for refletance from a semi-infinite turbid medium. J Opt Soc Am A 1997;14:246–54.
30. Hull EL, Nichols MG, Foster TH. Localization of luminescent inhomogeneities in turbid media with spatially resolved measurements of CW diffuse luminescence emittance. Appl Opt 1998;37:2755–65.
31. Hull EL, Nichols MG, Foster TH. Quantitative broadband near-infrared spectroscopy of tissue-simulating phantoms containing erythrocytes. Phys Med Biol 1998;43: 3381–404.
32. Choe R, Durduran T, Yu G, et al. Transabdominal near infrared oximetry of hypoxic stress in fetal sheep brain in utero. Proc Natl Acad Sci USA 2003;100:12950–4.
33. Culver JP, Durduran T, Furuya D, et al. Diffuse optical tomography of cerebral blood flow, oxygenation and metabolism in rat during focal ischemia. J Cereb Blood Flow Metab 2003;23:911–24.
34. Durduran T, Choe R, Culver JP, et al. Bulk optical properties of healthy female breast tissue. Phys Med Biol 2002;47:2847–61.
35. Corlu A, Durduran T, Choe R, et al. Uniqueness and wavelength optimization in continuous-wave multispectral diffuse optical tomography. Optics Letters 2003;28: 2339–41.
36. MacDonald IJ, Dougherty TJ. Basic principles of photodynamic therapy. J Porphyrins Phthalocyanines 2001;5:105–29.
37. Koch CJ. Oxygen sensor design: analysis and correction of problems associated with zero current, stability and structure. Adv Exp Med Biol 2003;510:151–6.
38. Hosmer DW, Lemeshow S. Applied survival analysis: regression modeling of time to event data. New York: John Wiley and Sons Inc., 1999.
39. Ihaka R, Gentleman R. R: a language for data analysis and graphics. J Computational and Graphical Statistics 1996;5:299–314.
40. Efron B, Tibshirani RJ. An introduction to the bootstrap. New York: Chapman and Hall; 1993.
41. Hull EL, Conover DL, Foster TH. Carbogen-induced changes in rat mammary tumor oxygenation reported by near infrared spectroscopy. Br J Cancer 1999;79:1709–16.
42. Cheung C, Culver JP, Takahashi K, Greenberg JH, Yodh AG. In vivo cerebrovascular measurement combining diffuse near-infrared absorption and correlation spectroscopies. Phys Med Biol 2001;46:2053–65.
43. Mitra S, Foster TH. Carbogen breathing significantly enhances the penetration of red light in murine tumours in vivo. Phys Med Biol 2004;49:1891–904.
44. Conover DL, Fenton BM, Foster TH, Hull EL. An evaluation of near infrared spectroscopy and cryospectrophotometry estimates of haemoglobin oxygen saturation in a rodent mammary tumour model. Phys Med Biol 2000;45:2685–700.
45. Durduran T, Yu G, Zhou C, et al. Diffuse optical measurements of blood flow, blood oxygenation and metabolism in human brain during sensorimotor cortex activation. Optics Letters 2004;29:1766–8.
46. Menon C, Polin GM, Prabakaran I, et al. An integrated approach to measuring tumor oxygen status using human melanoma xenografts as a model. Cancer Res 2003;63: 7232–40.
47. Gray LH, Steadman JM. Determination of the oxyhaemoglobin dissociation curves for mouse and rat blood. J Physiol 1964;175:161–71.
48. Coutier S, Bezdetnaya LN, Foster TH, Parache RM, Guillemin F. Effect of irradiation fluence rate on the efficacy of photodynamic therapy and tumor oxygenation in meta-tetra (hydroxyphenyl) chlorin (mTHPC)-sensitized HT29 xenografts in nude mice. Radiat Res 2002;158:339–45.
49. Sokolov VE. Mammal skin. Berkeley Los Angeles London: University of California Press; 1982.

50. Henderson BW, Fingar VH. Relationship of tumor hypoxia and response to photodynamic treatment in an experimental mouse tumor. Cancer Res 1987;47:3110–4.
51. Fingar VH, Wieman TJ, Park YJ, Henderson BW. Implications of a pre-existing tumor hypoxic fraction on photodynamic therapy. J Surg Res 1992;53:524–8.
52. Rofstad EK, Fenton BM, Sutherland RM. Intracapillary HbO2 saturations in murine tumours and human tumour xenografts measured by cryospectrophotometry: Relationship to tumour volume, tumour pH and fraction of radiobiologically hypoxic cells. Br J Cancer 1988;57:494–502.
53. Srinivasan S, Pogue BW, Jiang S, et al. Interpreting hemoglobin and water concentration, oxygen saturation, and scattering measured in vivo by near-infrared breast tomography. Proc Natl Acad Sci USA 2003;100:12349–54.
54. Cheung R, Solonenko M, Busch TM, et al. Correlation of in vivo photosensitizer fluorescence and photodynamic-therapy-induced depth of necrosis in a murine tumor model. J Biomedical Optics 2003;8:248–52.
55. Niedre MJ, Secord AJ, Patterson MS, Wilson BC. In vitro tests of the validity of singlet oxygen luminescence measurements as a dose metric in photodynamic therapy. Cancer Res 2003;63:7986–94.
56. Pogue BW, Pitts JD, Mycek M-A, et al. In vivo NADH fluorescence monitoring as an assay for cellular damage in photodynamic therapy. Photochem Photobiol 2001; 74:817–24.
57. Bremner JC, Wood SR, Bradley JK, et al. ^{31}P magnetic resonance spectroscopy as a predictor of efficacy in photodynamic therapy using differently charged zinc phthalocyanines. Br J Cancer 1999;81:616–21.
58. Nishiwaki M, Fujise Y, Yoshida TO, Matsuzawa E, Nishiwaki Y. Evaluation of the effects of photodynamic therapy with phosphorus 31 magnetic resonance spectroscopy. Br J Cancer 1999;80:133–41.
59. Gross S, Gilead A, Scherz A, Neeman M, Salomon Y. Monitoring photodynamic therapy of solid tumors online by BOLD-contrast MRI. Nat Med 2003;9:1327–31.